

Validation of a polarized hyperspectral imaging (PHSI) probe using phantoms and biological tissues

Ling Ma ^{a,b}, Amie Ha ^{a,b}, Izabella Cheverra ^{a,b}, Mandy Yuan ^{a,b}, Suhani Swain ^{a,b}, Baowei Fei ^{a,b,c*}

^a Center for Imaging and Surgical Innovation, University of Texas at Dallas, Richardson, TX

^b Department of Bioengineering, University of Texas at Dallas, Richardson, TX

^c Department of Radiology, University of Texas Southwestern Medical Center, Dallas, TX

*Corresponding author: bfei@utdallas.edu, Website: <https://fei-lab.org>

ABSTRACT

Polarized hyperspectral imaging (PHSI) combines wavelength-resolved reflectance with polarization sensitivity to probe tissue absorption, scattering, and microstructural organization in a label-free manner. We developed a compact handheld PHSI probe that integrates two liquid crystal variable retarders (LCVRs), a linear polarizer, and a hyperspectral snapshot camera to achieve full Stokes imaging over the range of 460–600 nm. In this work, we establish a comprehensive calibration and validation framework for this probe to improve its quantitative spectral and polarization performance. Individual LCVRs were first calibrated at four wavelengths (480, 530, 580, and 633 nm) using a crossed-polarizer method to obtain voltage–retardance characteristic curves and to determine the driving voltages corresponding to 0, $\lambda/4$, and $\lambda/2$ retardance at 530 nm. We then adapted a full-Stokes polarimeter calibration method to identify systematic errors at 520 nm, using six calibration samples and a Stokes–Mueller model that account for LCVR axis offsets, residual retardance errors, and polarizer misalignment. Spatial and spectral performance were evaluated using a USAF target, a ruler, and eight color tiles with known reflectance spectra, resulting in a field of view of 7 mm \times 11 mm, a resolution of 7.13 lines per millimeter (lp/mm), and spectral angles below 5°. Additional validation on Intralipid–dye phantoms and *ex vivo* mouse tissues demonstrated that the calibrated probe could capture dye- and tissue-specific reflectance and degree of polarization spectra. These results highlight the potential of the calibrated handheld PHSI probe as a portable tool for quantitative tissue characterization in biomedical research and diagnostics.

Keywords: polarized hyperspectral imaging (PHSI), probe, validation, phantom, tissue

1. INTRODUCTION

Quantitative optical imaging methods that exploit both spectral and polarization information can reveal subtle changes in tissue structure, composition, and organization without the need for exogenous contrast agents. Polarized hyperspectral imaging (PHSI) is one such technique, combining wavelength-resolved reflectance measurements with polarization sensitivity to probe absorption, scattering, and microstructural anisotropy in a spatially resolved manner.¹ ² By analyzing the wavelength dependence of Stokes parameters and derived polarization metrics, PHSI can provide rich contrast related to chromophore distributions and tissue architecture that is not accessible with conventional intensity-only imaging.

For PHSI systems based on liquid crystal variable retarders (LCVRs), accurate recovery of the Stokes vector relies critically on precise knowledge of the polarization states generated by the modulator at each wavelength. In practice, LCVR retardance depends on both driving voltage and wavelength, and may deviate from nominal 0, $\lambda/4$, or $\lambda/2$ values in a state- and wavelength-dependent manner.³ Additional imperfections in polarizers, optics, and alignment further contribute to systematic errors in the measured spectra and polarization signatures. If these effects are not properly characterized and corrected, they can lead to biased Stokes reconstruction, distort spectral features, and compromise the reliability of downstream tissue analysis, especially when comparing measurements across wavelengths, samples, or instruments.

Our group previously developed a compact, handheld PHSI probe with full Stokes imaging capability and demonstrated its use on phantoms and *ex vivo* mouse tissues for assessing burn injury and differentiating tissue types based on spectral and polarization contrast.^{2,4} In those studies, the primary focus was on demonstrating feasibility and exploring intrinsic contrast mechanisms. As the probe moves toward quantitative biomedical applications, systematic calibration and thorough validation of spectral fidelity and polarization accuracy become essential.

In this work, we present a calibration and validation framework for our handheld PHSI probe. We first perform calibration of each individual LCVR to obtain its retardance characteristic curves at different wavelengths. Considering the intrinsic residual retardance error and axial offset, we measured the systematic errors at 520 nm and modeled them using non-linear fitting for error correction. Next, polynomial models of state- and wavelength-dependent spectral errors were incorporated into a post-processing correction scheme for improved Stokes parameter estimation. We evaluate the resulting spectral accuracy using color tiles with known reflectance spectra and further validate the corrected system on dye-loaded lipid emulsion-agar phantoms, where both reflectance trends and degree of polarization (DOP) spectra can be compared with expected absorption behavior. Finally, we apply the calibrated probe to freshly excised mouse tissues from multiple organs to assess its ability to capture distinct absorption and polarization signatures in a biologically relevant setting. Together, these studies establish a robust methodology for calibrating LCVR-based PHSI systems and demonstrate the enhanced performance of a portable PHSI probe for quantitative tissue characterization.

2. METHODS

PHSI Probe

To improve the usability and portability of the PHSI imaging system, we designed the optics and mechanics into a lightweight, fully handheld probe, as described in our earlier work.² Illumination was provided by a compact ring light combined with a ring-shaped linear polarizer (LP) mounted at the distal tip of the probe. The imaging path consisted of two LCVRs, an LP, and a lens in front of a hyperspectral snapshot camera attached at the proximal end. By stepping through a sequence of LCVR driving voltages, the system acquired four polarization-modulated intensity images that were later used to reconstruct the full Stokes vector.

The transmission axis of the illumination polarizer was oriented at 45°, while the analyzer polarizer in front of the camera was set to 0°. The fast axes of the first and second LCVRs were aligned at 0° and 45°, respectively, to enable effective polarization state modulation. All optical components were integrated into a 3D-printed housing with interfaces on both ends, allowing for the secure attachment of the ring light and the camera. Custom control software, built on the application programming interfaces (APIs) of the LCVRs and hyperspectral camera, coordinated voltage modulation and image acquisition. The software supported automatic acquisition of the four polarization states and data processing.

Calibration of LCVR retardance characteristics

The LCVRs were calibrated to establish voltage–retardance relationship using the crossed polarizers method.⁵ Due to the wavelength-dependent characteristics of the LCVR, calibration must be performed at individual wavelengths. Thus, a filter wheel with four different filters was placed in front of a xenon white light source to provide close-to-monochrome illumination. Considering the wavelength range of our probe (460-600 nm), we selected three filters at the short end (480 nm), middle (530 nm), and long end (580 nm) of the range. A 633 nm filter was also included in comparison with the manufacturer's reference calibration data.

Each LCVR was calibrated at four wavelengths separately to obtain the power-voltage characteristic curves. We swept the LCVR driving voltage from 0.1 V to 10 V at an increment of 0.1 V and recorded the power meter reading at each step. Then, the power meter readings were normalized to a range of 0 to 1, which were converted and unwrapped to recover the retardance⁶ in both the degree and nm units. The retardance discrepancy among the three curves was evaluated, and the 633 nm retardance curve was compared with the manufacturer's reference. Eventually, the driving voltages for 0, $\lambda/4$, and $\lambda/2$ retardance based on $\lambda=530$ nm were selected for data acquisition, as it corresponds to the midpoint of the entire wavelength range.

Modeling and correction of the LCVR systematic errors

Our PHSI probe is capable of full Stokes imaging based on intensity measurements. However, variations of optical axis positions and retardance values can distort both the reconstructed Stokes parameters and the derived polarization metrics. To reduce these errors, we adapted a previously reported calibration strategy³ for LCVR-based full-Stokes polarimeters to identify systematic errors and correct them through postprocessing. All measurements were performed at a wavelength of 520 nm, which was a widely available laser option close to the midpoint of our PHSI spectral range. The calibration setup consisted of a linearly polarized laser beam incident on an LP with its transmission axis fixed at 45°. The transmitted beam then passed through a polarization calibration sample and reached the first measurement plane, where we recorded the light intensity for normalization later. Downstream this plane, the beam entered the Stokes polarimeter, which comprised LCVR 1 (fast axis oriented at 0°), LCVR 2 (fast axis at 45°), and an LP oriented at 0°, followed by a power meter placed at measurement point 2. The power meter was alternately positioned at measurement point 1 and measurement point 2 to record the transmitted intensity at each stage of the calibration procedure.

Polarization calibration samples were used to generate a broad set of known input states, including an LP, a quarter-wave plate (QWP), and a half-wave plate (HWP), with their transmissive/fast axes oriented at specific angles. For each sample, LCVRs were given different driving voltages, and the power meter readings were recorded.^{1, 3} Next, following the general approach,³ theoretical values and the resulting intensity responses were fit with a Stokes–Mueller forward model using nonlinear least-squares optimization. System error parameters were estimated, including the optical axis orientation of all components, and the retardance errors of the LCVRs at different retardance values. The fitted parameters were then incorporated into the Stokes reconstruction used in phantom and tissue experiments to compensate for systematic errors.

Validation of the spatial and spectral performance

For spatial performance validation, we imaged a ruler and a USAF-1951 target. Results show a field of view of 7 mm x 11 mm, as well as a decent resolution of 7.13 lp/mm. Regarding spectral fidelity, we imaged eight different color tiles with known reference spectra. Spectral angle was used as the metric to evaluate the discrepancy between measured and the reference reflectance spectra. A lower spectral angle indicates a higher spectral accuracy.

Validation of the PHSI probe on homemade Intralipid-dye phantoms

Intralipid-agar phantoms with different dyes were made in the lab for probe validation. The oil particles in Intralipid are the major scattering agent, while the dyes serve as absorbing agents. Four dyes with different absorption profiles were used, including crystal violet (violet), methylene blue (blue), tartrazine (yellow), and safranin (red). Phantoms with the same dye but different concentrations were also made to evaluate the probe's ability to detect different depolarization levels. For each phantom, four images (I_H , I_V , I_{45} , and I_{RC}) were acquired, from which Stokes vectors were calculated and degree of polarization was derived.

Validation of the PHSI probe on ex vivo mouse tissues

Six organs, i.e., brain, tongue, thyroid, skin, lung, and testicles, were excised from three euthanized mice and imaged using the PHSI probe. Spectral signatures of both reflectance and degree of polarization were retrieved and compared to evaluate the capability of the probe to differentiate tissues. In addition, the consistency across three mice were evaluated to prove the probe's stability.

3. RESULTS

LCVR calibration and wavelength-dependent error modeling

The retardance characteristics of one LCVR calibrated at 480 nm, 530 nm, 580 nm, and 633 nm are shown in Figure 1. The raw power–voltage curves (Fig. 1a) exhibit the expected oscillatory behavior as the applied voltage is swept. After normalizing transmittance (Fig. 1b), converting the normalized intensity to wrapped retardance (Fig. 1c), and applying the two-step unwrapping procedure, the unwrapped retardance increases monotonically with voltage, producing smooth retardance–voltage curves for all four wavelengths, as shown in Fig. 1(e-f). Minor discrepancies among the curves indicate the wavelength-dependent dispersion of the LCVR. From the 530 nm calibration curve, which corresponds to the midpoint of the probe's spectral range, we determined the driving voltages for nominal 0,

$\lambda/4$, and $\lambda/2$ retardance and used these values for subsequent imaging experiments. The 633 nm curve shows good agreement with the manufacturer’s reference, confirming the reliability of our calibration procedure.

Using these retardance–voltage relationships as a basis, we next applied the systematic error calibration at 520 nm to quantify residual axis offsets and retardance errors. The nonlinear fit to the intensity measurements from six calibration samples converged robustly, and the best-fit model reproduced the measured intensities with low residual error, indicating that the Stokes–Mueller model captures the dominant sources of systematic error in the system. The recovered parameters revealed small but non-negligible deviations of the LCVR fast-axis orientations from their nominal values and nonzero diattenuation for both LCVRs, in agreement with previous characterizations of similar devices. Incorporating these parameters into the forward model ensures that the four acquisition modes (I_H , I_V , I_{45} , and I_{RC}) are correctly interpreted during Stokes reconstruction, rather than assuming ideal retarders and perfectly aligned optics.

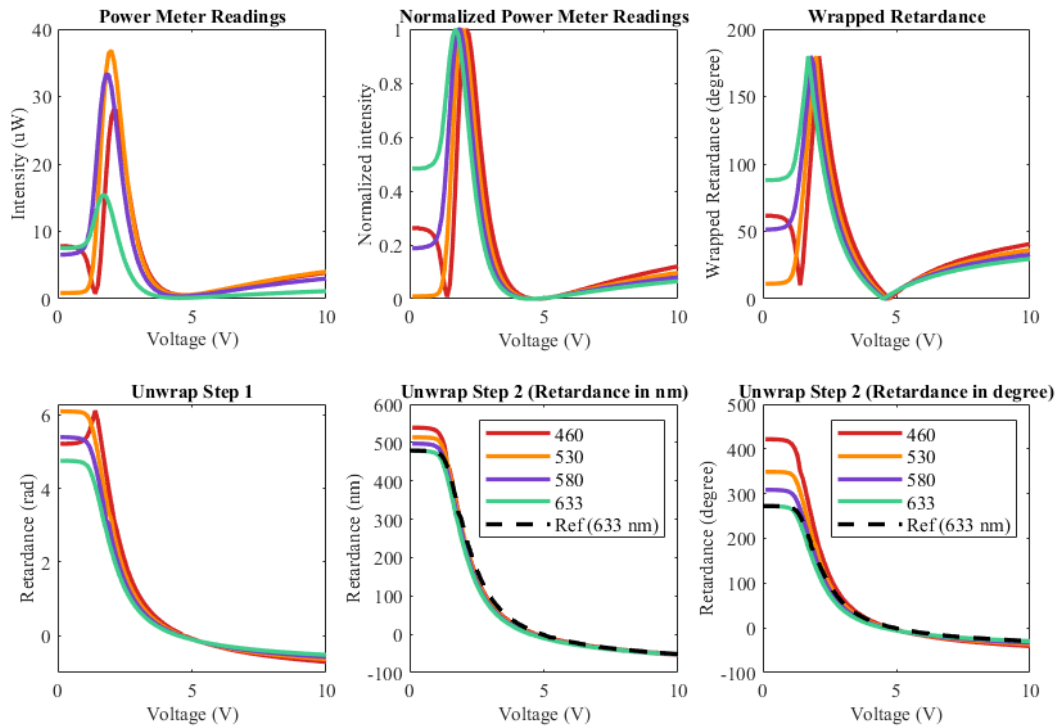


Figure 1. LCVR calibration results. (a) Power meter readings. (b) Normalized power meter readings in the range of 0 to 1. (c) Converted power meter readings to retardance but in the range of 0 to 180. (d) Unwrap step 1 results, retardance in the rad unit. (e) Retardance characteristic curves of a LCVR after unwrap step 2, calibrated at 480 nm, 530 nm, 580 nm, and 633 nm. (f) Retardance characteristic curves of a LCVR in the unit of degree. Dashed line is the reference calibration curve from the manufacturer.

Spectral validation on color tiles

Figure 2 shows the spectral performances of the probe on eight color tiles with known reflectance spectra. The color images are HSI-synthetic RGBs extracted from the center of the tiles. Note that the colors of the violet, purple, and red tiles are off because our HSI camera did not cover most of the red spectral bands. Considering the Stokes vectors and degree of polarization are derived from measured reflectance spectra, it is critical for the probe to retrieve accurate reflectance information of the target. It can be seen that for all 8 color tiles, the probe yielded a satisfying spectral accuracy with spectral angles lower than 5° .

Validation on Intralipid-dye phantoms

Figure 3 shows the spectral performances of the probe on homemade Intralipid-dye phantoms. It can be seen that the reflectance spectra from all four images (I_H , I_V , I_{45} , and I_{RC}) closely resemble the absorption profile of the respective

dye. The DOP spectra are distinctly impacted by the dyes, with the peak DOP values correspond with dye absorption maxima. In addition, with the increase of dye concentration, i.e., increase in absorption, the probe revealed decreased reflectance as well as increased DOP.

Validation on *ex vivo* mouse tissues

Figure 4 shows the reflectance and DOP spectra of six different organs from three mice. Each organ exhibits distinct spectral signatures related to the different compositions of chromophores and scattering components. The shape and magnitude of both reflectance and DOP spectra could serve as features for tissue differentiation.

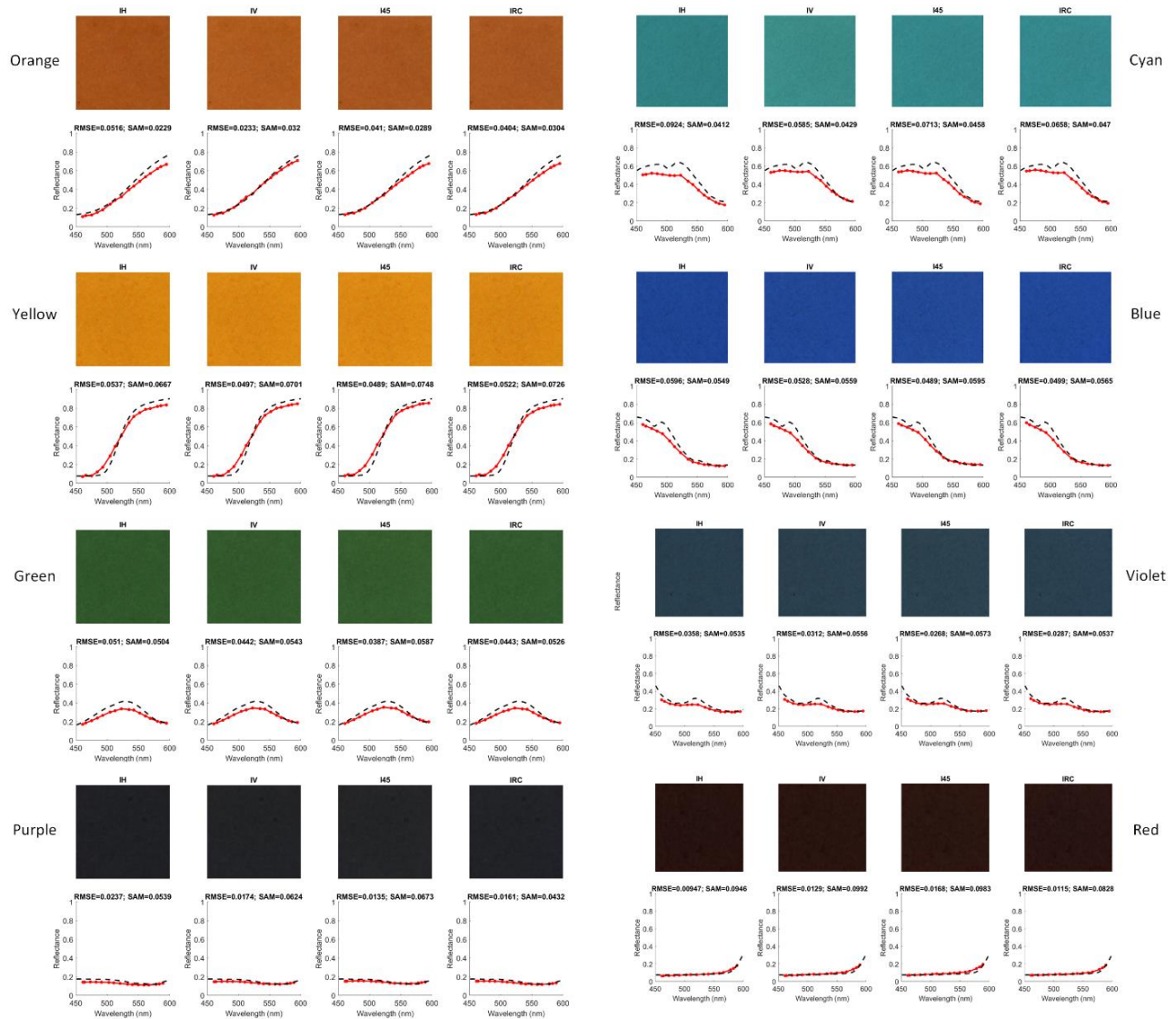


Figure 2. Validation of the PHSI probe's spectral accuracy on standard color tiles.

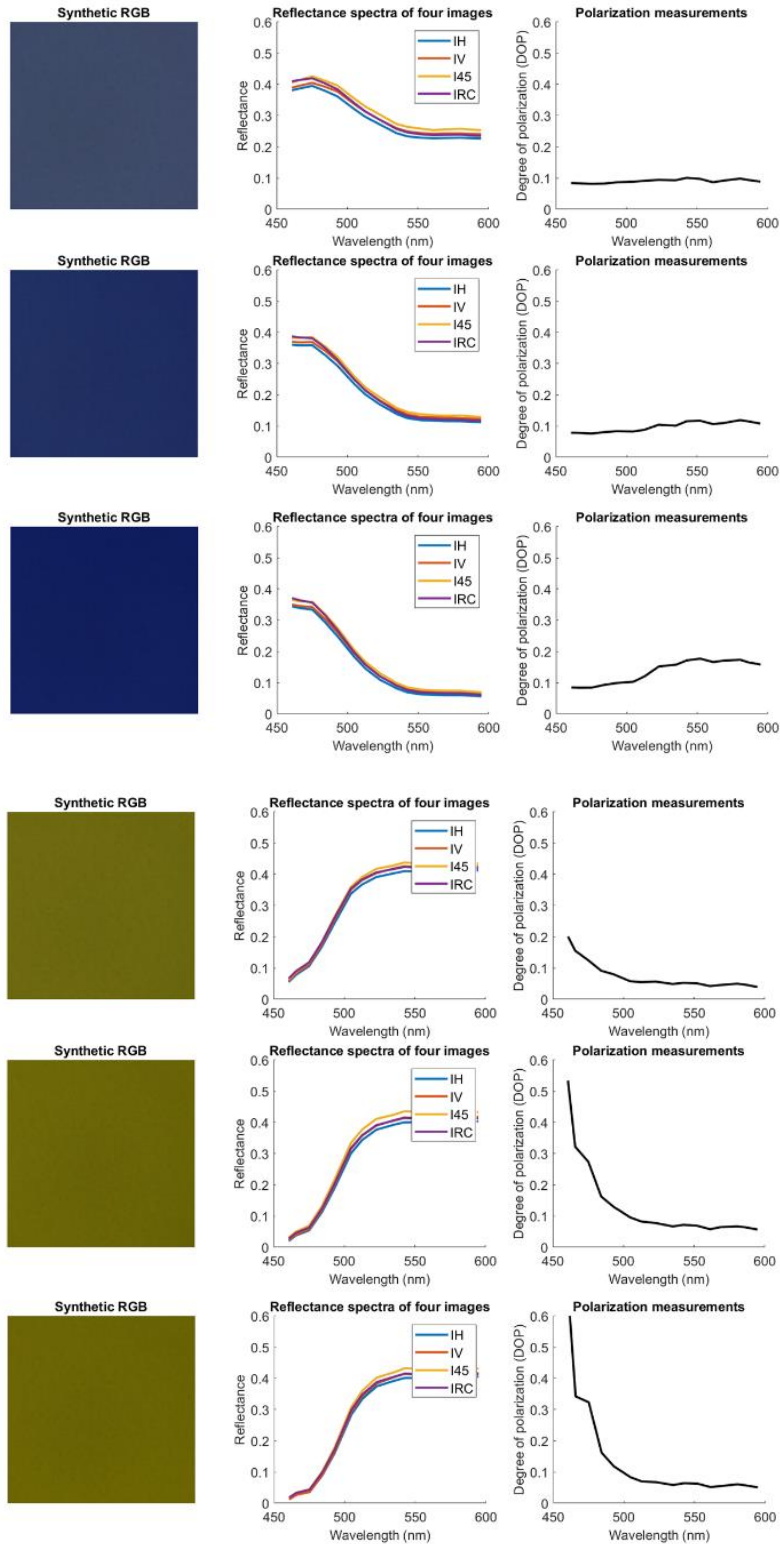


Figure 3. Reflectance and degree of polarization spectra of Intralipid-dye phantoms measured by the PHSI probe. Left: Crystal violet. Right: Tartrazine. From top to bottom: low, medium, and high concentrations of the dye.

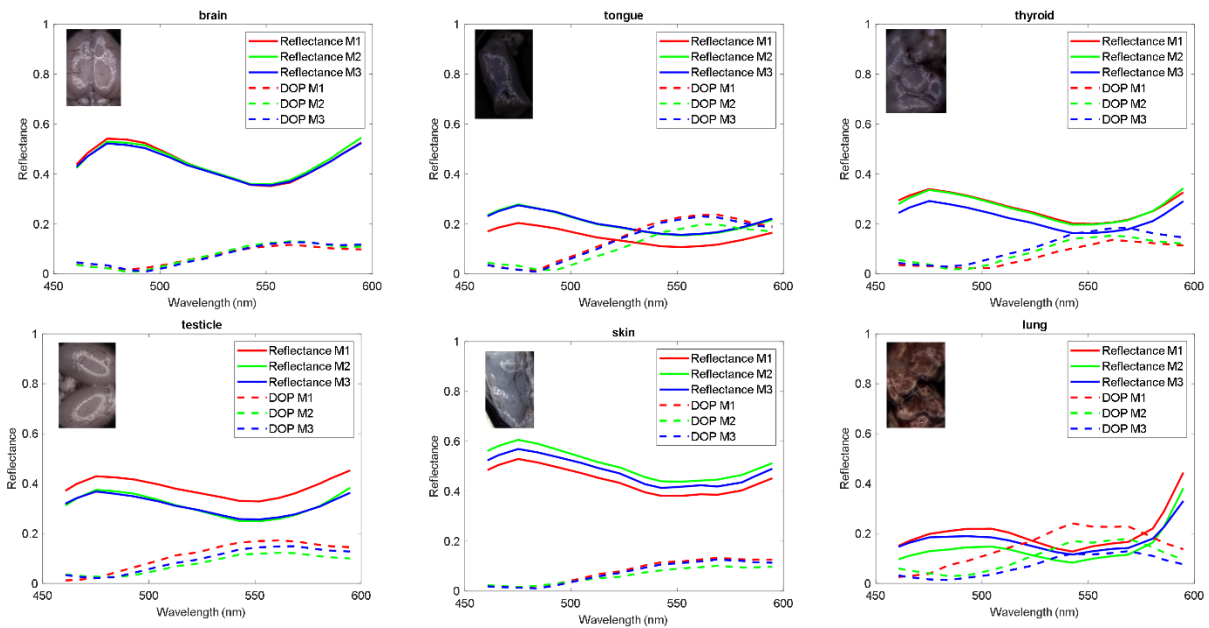


Figure 4. Spectral signatures of reflectance and degree of polarization of six organs from three mice.

4. CONCLUSION AND DISCUSSION

In this work, we established a systematic validation framework for a handheld PHSI probe and demonstrated its capability for quantitative spectral and polarization measurements on phantoms and biological tissues. We first characterized the retardance–voltage behavior of each LCVR at multiple wavelengths. Then, we adopted a full-Stokes calibration method based on variable retarders to correct systematic errors, particularly related to the orientation and retardance of the LCVRs. We substantially reduced instrument-induced distortions in both reflectance and polarization signals. The resulting system combines the portability of a compact probe with the quantitative performance required for reliable tissue characterization.

The validation experiments further illustrate the impact of this calibration on practical imaging performance. Measurements on standard color tiles demonstrated that the calibrated probe accurately reproduces the reference reflectance spectra, with spectral angles of less than 5° , indicating high spectral fidelity across the operating wavelength range. This is a critical requirement, as both the Stokes vector and polarization metrics are computed from the underlying reflectance spectra, and any systematic spectral bias would propagate directly into the polarization domain. The Intralipid–dye phantom results demonstrate that the probe not only captures reflectance trends consistent with the known absorption profiles of each dye but also reveals dye-specific DOP spectra whose peaks coincide with the absorption maxima. The observed decrease in reflectance and increase in DOP with higher dye concentration suggest that the probe is sensitive to coupled changes in absorption and multiple scattering, and that polarization contrast can provide complementary information beyond intensity alone.

Ex vivo imaging of multiple mouse organs further confirms the potential of the calibrated PHSI probe for tissue differentiation. Each organ exhibited distinct reflectance and DOP spectra, reflecting differences in chromophore composition, microstructure, and scattering anisotropy. The qualitative consistency of these signatures across three animals supports the stability of the probe and the robustness of the calibration procedure. Although the present study focused on a limited set of organs and *ex vivo* samples, the clear separation of spectral–polarimetric features across tissue types suggests that combining reflectance and polarization information may enable classification schemes or quantitative models for tissue assessment in future work.

Several limitations of this study should be acknowledged. First, all biological measurements were performed on *ex vivo* tissues. Additional work is needed to evaluate probe performance under *in vivo* motion, hemodynamics, and heterogeneous illumination. Second, we focused on Stokes-based metrics such as DOP rather than full Mueller matrix analysis, which could provide richer information about depolarization and anisotropy. Finally, the current analysis was performed offline; real-time implementation of the calibration and reconstruction pipeline, coupled with automated feature extraction and classification, will be important for intraoperative or point-of-care deployment.

Overall, we demonstrated that a compact, handheld PHSI system can provide quantitative spectral and polarization measurements suitable for tissue characterization in a laboratory setting. The combination of portability, full-Stokes capability, and improved calibration positions the probe as a promising platform for future biomedical applications, including burn assessment, tissue differentiation, and potentially image-guided surgery. Ongoing and future work will focus on investigating various spectral ranges, implementing real-time data processing, and translating the calibrated PHSI probe for use in *in vivo* preclinical and clinical studies.

ACKNOWLEDGMENTS

Research reported in this publication was supported in part by the National Cancer Institute of the National Institutes of Health under Award Number R01CA288379 and R01CA204254 and by the Cancer Prevention and Research Institute of Texas (CPRIT) under Award Number RP240289 and RP240542. The content is solely the responsibility of the authors and does not necessarily represent the official views of the National Institutes of Health.

DISCLOSURES

The authors have no relevant financial interests in this article and no potential conflicts of interest to disclose.

REFERENCES

- [1] Ma, L., Srinivas, A., Krishnamurthy, A., Zhou, X., Shah, N. S., Obaid, G., and Fei, B., "Automated polarized hyperspectral imaging (PHSI) for ex-vivo and in-vivo tissue assessment." Proc. SPIE 12391, 123910F (2023).
- [2] Sherey, J., Ma, L., Ha, A., Lane, C., and Fei, B., "Validation of a handheld polarized hyperspectral imaging probe on intralipid phantom and mouse tissue." Proc. SPIE 13322, 1332204 (2025).
- [3] Montes-González, I., Bruce, N. C., Rodríguez-Herrera, O. G., and Rodríguez Núñez, O., "Method to calibrate a full-Stokes polarimeter based on variable retarders," Applied Optics, 58(22), 5952-5957 (2019).
- [4] Ma, L., Chaverra, I. M., Patwardhan, C., Swain, S., Rudro, R., and Fei, B., "Validation of a polarized hyperspectral imaging (PHSI) probe using phantoms and biological tissues." Proc. SPIE 13854(2026).
- [5] Gilman, S., Baur, T., Gallagher, D., and Shankar, N., "Properties Of Tunable Nematic Liquid Crystal Retarders." Proc. SPIE 1166 (1990).
- [6] López-Téllez, J. M., and Bruce, N. C., "Stokes polarimetry using analysis of the nonlinear voltage-retardance relationship for liquid-crystal variable retarders," Review of Scientific Instruments, 85(3), (2014).